Development of Radiation Tolerant Monolithic Active Pixel Sensors With Fast Column Parallel Read-Out.

M. Koziel*[,a], A. Dorokhov[a], J.-C. Fontaine[b], R. De Masi[a], M. Winter[a]

[a] *Institut Pluridisciplinaire Hubert Curien (IPHC), 23 rue de Loess, Strasbourg, France*
[b] *Groupe de Recherche en Physique des Hautes Energies (GRPHE), Mulhouse University, France*

Abstract

Monolithic Active Pixel Sensors (MAPS) [1] are being developed at IPHC - Strasbourg to equip the EUDET telescope [2] and vertex detectors for future high energy physics experiments, including the STAR upgrade at RHIC [3] and the CBM experiment at FAIR/GSI [4]. High granularity, low material budget and high read-out speed are systematically required for most applications, complemented, for some of them, with high radiation tolerance. A specific column-parallel architecture, implemented in the MIMOSA-22 sensor, was developed to achieve fast read-out MAPS. Previous studies of the front-end architecture integrated in this sensor, which includes in-pixel amplification, have shown that the fixed pattern noise increase consecutive to ionizing radiation can be controlled by means of a negative feedback [5]. However, an unexpected rise of the temporal noise was observed. A second version of this chip (MIMOSA-22bis) was produced in order to search for possible improvements of the radiation tolerance, regarding this type of noise. In this prototype, the feedback transistor was tuned in order to mitigate the sensitivity of the pixel to ionizing radiation. The performances of the pixels after irradiation were investigated for two types of feedback transistors: Enclosed Layout Transistor (ELT) [6] and "standard" transistor with either large or small transconductance. The noise performance of all test structures was studied in various conditions (expected in future experiments) regarding temperature, integration time and ionizing radiation dose. Test results are presented in this paper. Based on these observations, ideas for further improvement of the radiation tolerance of column parallel MAPS are derived.

Key words: radiation hardness, radiation tolerance, Monolithic Active Pixel Sensors, CBM, STAR, EUDET

1. Introduction

Efficient particle tracking in modern high energy physics experiments requires sensors with excellent performances regarding granularity and material budget, with mild compromises on the read-out speed and radiation tolerance. Monolithic Active Pixel Sensors (MAPS) offer an attractive solution for this kind of trade-off.

These sensors integrate the sensing elements and the processing electronics on the same substrate. Due to their thin sensitive volume, they can be thinned down to about 50 μm or even less, exposing low material budget to traversing particles. When the latter cross the detector volume, e-h pairs are generated along their trajectory. Electrons produced in the high resistivity p-type epitaxial layer diffuse thermally towards regularly implanted n-wells, where they are converted to voltage on the diode capacitance, and read out. Previous studies of MAPS in a 0.35 μm process have shown that those sensors meet well many of the requirements of upcoming or future high energy physics experiments. Typical performances achieved are a detection efficiency above 99.5% for an average fake hit rate below 10^{-4}, combined with a radiation tolerance of up to 1MRad of ionizing dose and 10^{13} n_{eq}/cm^2 fluence [7]. The radiation tolerance was assessed for sensors with a simple in-pixel architecture and a sequential, analogue rolling-shutter read-out. Realizing fast sensors imposed to implement signal processing micro-circuits inside each pixel. The main purpose of this paper is to summarize the achieved ionizing radiation tolerance for this new category of pixels.

Sequential MAPS read-out features a read-out speed basically proportional to the number of pixels. The maximum frequency which could be used for the chip read-out is limited by the parasitic capacitances which have to be recharged when switching from one pixel to the next. To speed up the read-out, sensors can be organized in N columns read out in parallel. This solution reduces the integration time by factor of N w.r.t. a fully sequential read-out. Moreover, the data flux produced by highly granular sensors with analogue output may easily become too large to be handled efficiently. In order to suppress the data stream from the sensor, a logic which selects, and sends information related to, pixels with signal above a certain threshold has to be implemented in the sensor.

*michal.koziel@ires.in2p3.fr

The development of fast MAPS was consequently organized in two parallel streams. One addressing the fast sensing part with a column parallel read-out architecture. The other stream covered the sparsification logic. The sensing part contains n-well diodes indicating the passage of particles and the signal processing circuitry (amplification and Correlated Double Sampling). The amplified signal samples are compared with a fixed threshold. This operation is performed via column level discriminators [8, 9].

To search for the best in-pixel amplifier structure, several alternatives were studied with the MIMOSA-22 chip. As compared to previous prototypes, MIMOSA-22 provided for the first time opportunities to study the radiation tolerance of sensors with in-pixel signal processing circuitry. This paper summarizes the radiation tolerance assessment for this device. In general, the signal processing circuitry showed sensitivity to ionizing doses, which translated eventually into detection efficiency losses. A second version of this chip - MIMOSA-22bis - was produced to explore in-pixel amplifier architectures expected to be more robust against damage introduced by ionizing particles.

2. In-pixel amplifiers and their radiation tolerance assessment – MIMOSA-22

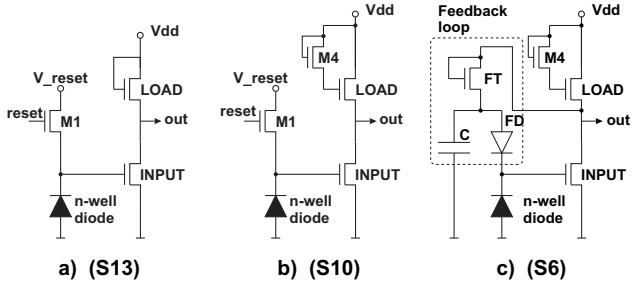

Figure 1: *In-pixel amplifier architectures included and tested with MIMOSA-22: a) Common Source (CS) amplifier, b) CS amplifier with improved gain, c) CS amplifier with improved gain and negative feedback loop.*

In order to combine the fast column parallel read-out and the data sparsification, some modifications to ordinary CMOS pixels are needed. The signal produced by impinging particles is relatively small and only a fraction of it is available on the seed pixel. For a sensing diode size of $4.3 \times 3.4\ \mu m^2$, the Most Probable Value (MPV) of the charge collected in the seed pixel is around 200 - 300 electrons. Assuming 8 - 10 fF for the diode capacitance and including the other parasitic capacitances, e.g. the capacitance of the source follower, the signal is in the range of 3.5 - 4.5 mV. Moreover, the diode output voltage has some offset which varies from one diode to another. The standard deviation of the offset/pedestal distribution is called Fixed Pattern Noise (FPN). FPN originates from the accuracy and reproducibility of the CMOS fabrication processes. This feature manifests itself in the mask production, doping concentrations, contamination during fabrication, characteristics of MOSFETs (Vt, gain, W, L, etc.). In order to select pixels delivering a signal above a certain level, the signal samples have to be compared with a discriminator threshold voltage. To accommodate the small pixel pitch, the comparators are moved outside of the pixel area. A single comparator is therefore used for each of the columns. As the magnitude of the FPN may be in the same range as the signal generated by an impinging particle [8], the signal selection with the column discriminator may become ineffective. To overcome this problem, signal amplification and FPN reduction have to be integrated in each pixel. In parallel, the temporal noise, having its origin in the sensing diode shot noise and in the in-pixel circuitry (transistor thermal, shot and 1/f noise), has to be kept as low as possible.

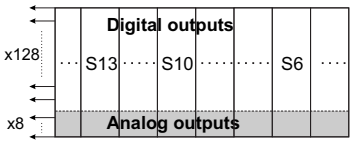

Figure 2: *Sketch of the overall architecture of MIMOSA-22/22bis, featuring 128 digital outputs and 8 analogue ones, and showing the position of sub-array S6, S10 and S13.*

In order to find the optimum in-pixel amplifier architecture, several options were studied with MIMOSA-22. They are sketched in Fig.1. The simplest one (S13), based on a Common Source (CS) amplifier, is shown in Fig.1(a). The same structure, but with an improved gain (S10), is represented by Fig.1(b). Fig.1(c) displays the architecture based on a CS amplifier stage with an improved gain complemented with a negative feedback loop (S6). The overall MIMOSA-22 architecture is sketched in Fig.2. The sensor is composed of 136 columns. 128 of those are ended with discriminators and deliver a binary output. The eight remaining columns are free of discrimination and provide therefore an analogue output allowing for pixel characterization.

Some sensors were irradiated with 10 keV X-Rays up to 300 kRad. They were consecutively characterized in the laboratory with an ^{55}Fe source. The FPN and the temporal noise were investigated. The FPN came out unchanged after irradiation (See Fig.3) for the structure S6, which features the improved gain and the feedback loop. This pixel design was therefore retained as a baseline for future sensors with column level signal discrimination. On the other hand, the temporal noise was observed to rise for all 3 amplifier architectures, which affected the detection efficiency, assessed later on with high energy pion beams at the CERN-SPS. The value of this noise component exceeded the one measured previously with pixels free of signal processing micro-circuits [10]. The currently

observed temporal noise increase could therefore not be attributed to the sensing diode, but rather to the in-pixel amplifier. This observation triggered the design of a modified MIMOSA-22 sensor, called MIMOSA-22bis.

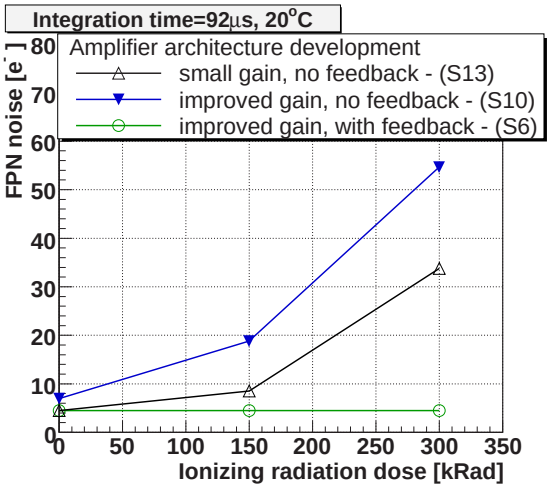

Figure 3: *The FPN of three different amplifier architectures included in MIMOSA-22.*

3. Radiation tolerance improvement – MIMOSA-22bis

The temporal noise increase after irradiation was suspected to originate from the feedback loop properties. Before irradiation, the feedback transistor and capacitance form a low pass filter with a relatively large time constant. All crosstalk signals coming from the rest of the in-pixel circuits, e.g. digital switches, are well filtered by the afore mentioned filter. Those signals are then not transferred through the feedback to the amplifier input and do not contribute to the noise. The DC potential of the sensing diode connected to the amplifier input being defined by the feedback, it remains stable.

After irradiation, the situation is different since the oxide properties are degraded. The dynamic resistance of the feedback transistor is decreased due to parasitic leakage current circulation between the drain and the source of the transistor. Consequently, the time constant of the low pass filter decreases and crosstalk signals may be partially transferred to the amplifier input, which may contribute significantly to the noise. Also, the amplifier input potential is changed due to the larger voltage drop on the feedback transistor. Because of the afore mentioned reasons, the properties of the feedback loop have to be studied in details.

It seems justified to upgrade the transistor in the feedback to its radiation tolerant enclosed layout version. This design choice, due to its relatively large parasitic capacitance, will increase the low pass filter time constant and consequently reduce its cut-off frequency, translating into a better filtering of unwanted signals reaching the diode through the feedback loop. The main advantage expected is that the afore mentioned time constant remains unchanged after irradiation. On the other hand, the amplifier structure with the feedback loop has a "memory" effect, since the current state depends on previous states. The solution with ELT introduces the risk that this memory effect will be enhanced by a larger time constant of the low pass filter. As a consequence, the voltage on the sensing diode will not be restored to its initial value between two consecutive read-outs (in case of impinging particle).

3.1. Tested sub-arrays

Table 1: *Feedback transistors used in test structures implemented in MIMOSA-22bis.*

Diode	Feedback trans.	Trans. dimensions
$4.3\times3.4\mu m^2$	ELT	W=4.4μm, L=0.35μm
$4.3\times3.4\mu m^2$	"standard"	W=0.4μm, L=0.5μm
$3.1\times3.65\mu m^2$	ELT	W=4.4μm, L=0.35μm
$3.1\times3.65\mu m^2$	"Weak"	W=0.4μm, L=1.05μm
$3.1\times3.65\mu m^2$	"Strong"	W=2.1μm, L=0.35μm

The approach mentioned above was investigated with several test structures implemented in MIMOSA-22bis, based on the same architecture as MIMOSA-22. Table 1 summarizes the characteristics of the feedback transistors implemented in each sub-array of MIMOSA-22bis. The ELT was implemented in the feedback loop of the in-pixel amplifier of two sub-arrays which differ in sensing diode size (4.3×3.4 μm^2 and 3.1×3.65 μm^2). The different diode sizes were used to identify the magnitude of the sensing diode shot noise component. The sub-matrix containing the "standard" feedback transistor was an exact copy of sub-array S6 tested previously with MIMOSA-22. It was used to compare the performance of the amplifier with feedback ELT to the feedback transistor used before. Two sub-arrays with smaller (3.1×3.65 μm^2) diodes were equipped with "weak" and "strong" feedback transistors. The latter were used for further verification of the influence of the transistor type and geometry on the in-pixel amplifier performance after irradiation.

4. Tests, results and discussion

4.1. Tests of sub-arrays with larger diodes

MIMOSA-22bis test matrices, which contain pixels equipped with diodes of 4.3×3.4 μm^2 as listed in Table 1, were tested at the CERN-SPS with a 120 GeV pion beam. The tests were performed with non-irradiated devices as well as with those exposed to integrated doses of 150 kRad and 300 kRad obtained with 10 keV X-Rays. The studies were performed at the nominal integration time of $\sim$92 μs, achieved with a 100 MHz read-out clock frequency, and at a stabilized temperature of 20 ^{o}C. The detection efficiency and the average fake hit rate ware

studied. The measured values of those parameters, for both sub-arrays irradiated up to 300kRad, were similar despite of the different feedback transistors used. This observation motivated further laboratory investigations.

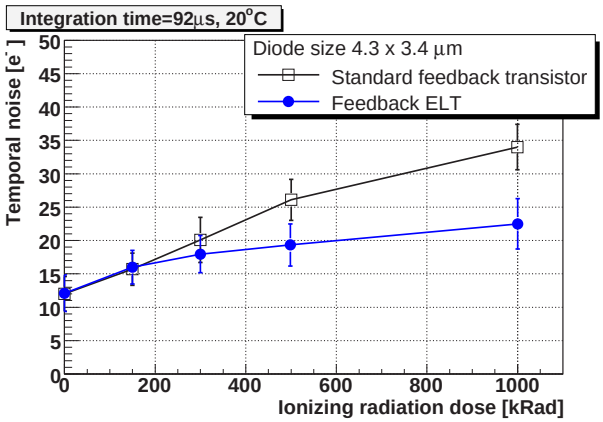

Figure 4: *Temporal noise as a function of ionizing dose for "standard" and enclosed layout feedback transistor.*

Extended tests covering a significant range of temperatures, irradiation doses and integration times were performed. The main parameter studied was the temporal noise, which was measured for sensors irradiated with doses of up to 1 MRad obtained with 10 keV X-Rays. Figure 4 shows how it varies with the ionizing dose for sub-arrays containing either a "standard" transistor or an ELT in the feedback loop. The observed temporal noise is nearly the same for both sub-arrays up to about 300 kRad. This confirms the afore mentioned observation made with a high energy pion beam. However, for higher integrated doses, the temporal noise of the sub-array based on a feedback ELT is lower than the one based on a "standard" transistor. E.g. after 1 MRad of integrated dose, the difference observed amounts to $\sim 12 \pm 3$ e$^-$.

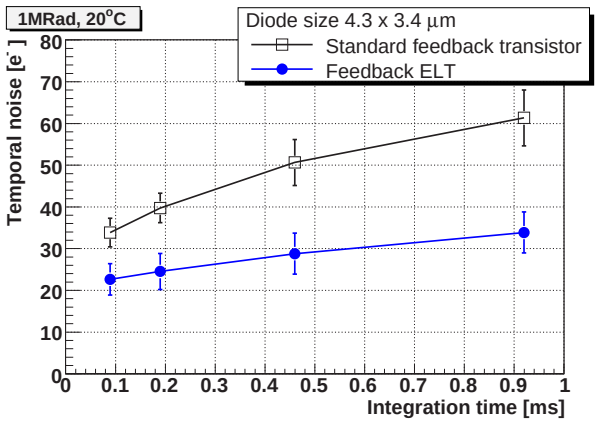

Figure 5: *Temporal noise as a function of integration time for "standard" and enclosed layout feedback transistors.*

Shortening the integration time resulted in a positive effect for all investigated designs, but substantial performance differences between the feedback ELT and the "standard" feedback transistor were still visible (see Fig.5). One may observe that the noise variations displayed in Fig.5 indicate that even a very short integration time would not allow reducing the temporal noise significantly below 20 e$^-$ in case of a 1 MRad integrated dose.

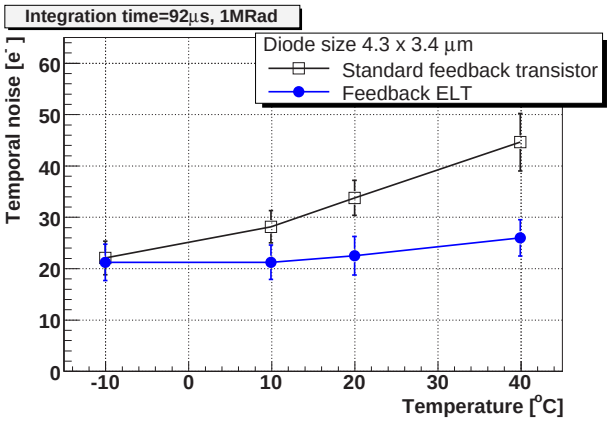

Figure 6: *Temporal noise as a function of temperature for "standard" and enclosed layout transistor in a feedback.*

The temporal noise was also studied in a wide temperature range, from - 10 ^{o}C to + 40 ^{o}C. It was observed that lowering the temperature to - 10 ^{o}C eliminates the performance difference between the "standard" transistor and the ELT feedback designs (see Fig.6). This observation points back to the diode leakage current, in contrast with what was concluded from measurements performed with "simple" pixels (see section 2).

For the lowest temperature used during the tests, the diode voltage decay due to the leakage current was limited and the amplifier operation point remained almost unchanged. For the highest temperature, the diode voltage decayed faster due to the leakage current increase. That decay was compensated by the negative feedback, and the efficiency of this compensation depended on the feedback transistor. The ELT feedback transistor came out to be the best choice. Nevertheless, after an integrated dose of 1 MRad and at a temperature of - 10 ^{o}C, a temporal noise of $\sim$22 e$^-$ was still observed (see Fig.6), well above the acceptable level of $\sim$15 e$^-$. The results indicated also that, at the lowest temperature considered, the noise component originating from the sensing diode leakage current was suppressed. The remaining temporal noise was similar for both, the "standard" and the enclosed feedback transistors. Consequently, the origin of the temporal noise excess observed should be attributed to other components of the in-pixel signal processing circuitry, besides the sensing diode and the feedback transistor.

4.2. Tests on sub-arrays with smaller diodes

The influence of the feedback transistor type and geometry on the temporal noise increase after irradiation was assessed in the same conditions as mentioned in the previous section. The temporal noise of sub-arrays containing smaller diodes (listed in Table 1) was investigated for integrated doses of up to 1 MRad. Its variations are displayed in Fig.7. It was observed that the ELT design was the best choice among the investigated feedback transistors, while the sub-array with the "strong" feedback transistor exhibited the worst performance.

This feature may be related to a change of the feedback low pass filter time constant. After ionizing radiation, leading to the accumulation of positive charges in the thick oxide, a parasitic path for leakage current is formed and allows charges to flow from the transistor source to its drain. As a consequence, the feedback low pass filter time constant may decrease. Thus, unwanted signals may not be filtered efficiently and since they could propagate to the amplifier input, they may contribute to the temporal noise increase. For the ELT version, almost no path for a parasitic current was created since the thin oxide (in which only a small amount of charges may be accumulated) surrounds the drain. Thus, the filter time constant was probably not strongly degraded in this case. The same explanation could also apply to the behaviour of sub-arrays with the "strong" and the "weak" feedback transistors. As the length of this parasitic path is proportional to the distance between drain and source, one may expect more parasitic current for short and wide transistor channels ("strong"). As a consequence, the time constant for the feedback low pass filter with the "strong" transistor was most degraded, resulting in a less efficient filtering of undesirable signals.

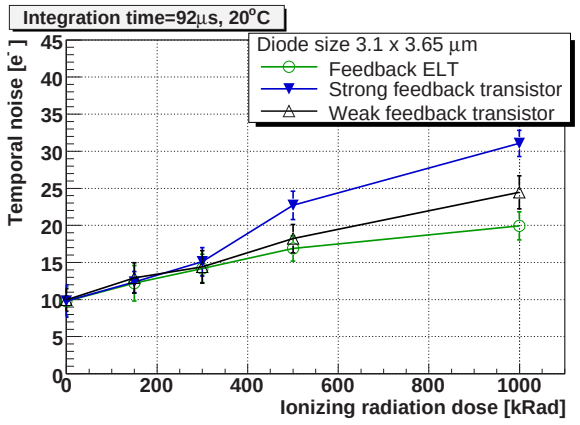

Figure 7: *Temporal noise as a function of ionizing dose for three investigated feedback transistors ("weak","strong",ELT).*

4.3. Additional observations

The measured temporal noise of the structures including feedback ELT with different n-well sizes indicates, that the diode shot noise contribution to the total temporal noise of the pixel is negligible (compare the temporal noise for sub-arrays containing the ELT in the feedback loop, Fig.4 and Fig.7).

The amplifier noise performance depends on the amplifier operation point. Due to radiation effects, which modify the transistor threshold voltage, the operation point may change consequently. The irradiated amplifier performance may be improved by compensating the shift of the amplifier bias point due to the threshold voltage change mentioned above. This can be obtained by modifying the DC potential transferred to the input transistor via the feedback loop. Such a modification can be done by changing the initial value of the transconductances for the load and the input transistors, thus the current flowing through them. The influence of both transistors' geometry (W/L) on the amplifier noise performance after irradiation was also addressed within MIMOSA-22bis. The tests have shown that modifying the transistor geometry had only a marginal effect on the pixel performance after irradiation.

5. Incoming test structures

The enclosed layout transistor architecture brought a noticeable improvement of performances for structures with negative feedback. Nevertheless, further studies have to be performed in order to meet the requirements of the most demanding applications in terms of radiation hardness (e.g. CBM experiment at FAIR). The noise level after an ionizing dose beyond ∼300 kRad is still above the expectation despite the use of the ELT in the feedback loop. Further improvements will come from a better understanding of other components. Better filtering of unwanted signals propagated through the feedback to the sensing diode could be achieved by implementing a larger feedback capacitance. A better separation of the signal from the noise could be realized with an amplifier providing a larger gain, e.g. based on a cascode configuration. Finally, the self-biased diode formed by a small p+ implant inside an n-well could be exchanged with an ELT working in diode configuration (see Fig.8). The ideas above are addressed within a new version of MIMOSA-22, labelled MIMOSA-22ter. The sensor was submitted to foundry in June 2009 and is expected back from fabrication in Autumn.

6. Read-out speed and the first full scale chip

The zero-suppression circuitry complementing the column parallel architecture implemented is the MIMOSA-22 prototypes, was developped with a stand-alone chip called SUZE-01 [11]. Its circuitry was adapted to 128 columns of pixels. Fabricated in 2007, it was extensively tested with millions of patterns and shown to work nominally up to 1.15 times its target clock frequency (100 MHz).

Finally, the MIMOSA-22 architecture and the zero suppression logic were combined in a full scale sensor (MIMOSA-26) manufactured in 2009. This device will equip the high resolution EUDET telescope, working in a rather moderate ionizing radiation environment. MIMOSA-26 is organized in 576 rows and 1152 columns, providing an active area of $\sim$2.2 cm^2. Despite its large number of pixels ($\sim$660 000), its zero suppression logic allows to run the sensor at a read-out frequency of $\sim$10 k frames/s. First test results show that, overall, the MIMOSA-22 and SUZE-01 performance are well reproduced. Extensive tests of this device are on-going in the laboratory, and will be complemented with 120 GeV pion beams at the CERN-SPS in September 2009.

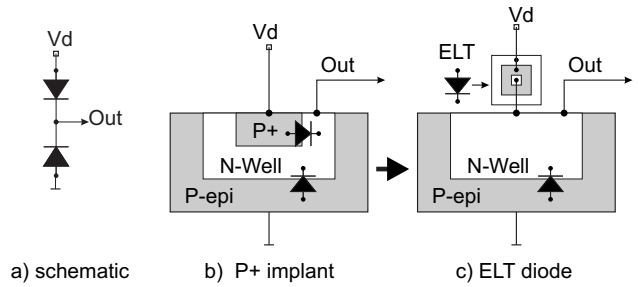

Figure 8: *Two implementation of a self biased pixel as sketched in (a): standard forwardly biased diode P+/N (b) and use of ELT (c).*

7. Summary - conclusions

This paper discussed the ionizing radiation tolerance of column parallel MAPS with in-pixel signal amplification. Three types of in-pixel amplifiers were investigated. The FPN was observed to remain unchanged, after irradiation up to several hundreds of kRad, using an amplifier equipped with negative feedback. After irradiation up to 300 kRad, the temporal noise increased above 15 e$^-$ENC, translating into a slight detection efficiency loss, showing that higher ionizing doses (e.g. 1 MRad as required for the CBM experiment) would presumably not be affordable. Based on previous studies, the rise of the temporal noise could not be attributed to the increase of the diode leakage current after irradiation. The investigations therefore concentrated on the in-pixel signal processing micro-circuitry. Looking for the components most sensitive to ionizing radiation, the influence of the feedback transistors characteristics on the amplifier noise performance was studied. Tests were performed at various temperatures and integration times. Sensors were irradiated up to 1 MRad and characterized. Among the different variants considered for the feedback transistor, the ELT came out as the most beneficial, especially for the highest doses, temperatures and integration times considered. The influence of the input and the load transistors on the amplifier noise performance after ionizing irradiation was also evaluated by changing their geometry. The impact of those transistors' geometry on the overall amplifier performance was however not significant. Overall, the radiation tolerance improvement obtained with the amplifier modifications investigated is still not sufficient for all applications of the sensors. Further improvement in ionizing radiation tolerance is therefore being addressed with alternative pixel designs recently submitted for production.

The first full scale chip, called MIMOSA-26, was produced. It combines the MIMOSA-22 architecture, which includes in-pixel signal processing and column-level discrimination, with a zero suppression logic and output memories. MIMOSA-26 meets well the requirements of the EUDET beam telescope, which may accumulate an integrated dose in the order of 100 kRad over 5 years of operation. In order to extend the field of applications of the sensor, such as a vertex detector component (e.g. STAR upgrade at RHIC or CBM at FAIR), the tolerance of the analogue part of the signal processing to ionizing radiation should still be improved. The necessary developments for this objective are under way.

References

[1] R. Turchetta et al., A monolithic active pixel sensor for charged particle tracking and imaging using standard VLSI CMOS technology, Nucl. Instr. & Meth. in Phys. Res. A 458 (2001), pp.677-689.

[2] T.Haas, A pixel telescope for detector R&D for an International Linear Collider, Nucl. Instr. & Meth. in Phys. Res. A 569 (2006), pp.53-56.

[3] The STAR Collaboration, Experimental and theoretical challenges in the search for the quark-gluon plasma: The STAR Collaboration's critical assessment of the evidence from RHIC collisions, Nucl. Instr. & Meth. in Phys. Res. A 757 (2005), pp.102-183.

[4] J.M.Heuser, Requirements for the Silicon Tracking System of CBM at FAIR, Nucl. Instr. & Meth. in Phys. Res. A 568 (2006), pp.258-262.

[5] Ch. Hu-Guo et al., Design and Characterisation of a Fast Architecture Providing Zero Suppressed Digital Output Integrated in a High Resolution CMOS Pixel Sensor for the STAR Vertex Detector and the EUDET Beam Telescope, TWEPP conference, Naxos, Greece, 15-19 September 2008, pp.80-84.

[6] W. Snoeys et al., Layout techniques to enhance the radiation tolerance of standard CMOS technologies demonstrated on a pixel detector read-out chip, Nucl. Instr. & Meth. in Phys. Res. A 439 (2000), pp.349-360.

[7] M. Deveaux, Design consideration for te Micro Vertex Detector of the Compressed Batyonic Matter experiment, in proceedings of 17th International Workshop on Vertex detectors, Sweden, July/August 2008. PoS(VERTEX 2008)028

[8] Y.Degerli., Design of fundamental building blocks for fast binary read-out CMOS sensors used in high-energy physics experiments, Nucl. Instr. & Meth. in Phys. Res. A 602 (2009), pp.461-466.

[9] G.Deptuch et al., Monolithic Active Pixel Sensors with in–pixel doule sampling operation and column–level discrimination, IEEE Trans. on Nucl. Science, vol. 51 (2004), pp.2313-2321

[10] M.Deveaux, PhD Thesis, Development of fast and radiation hard Monolithic Active Pixel Sensors (MAPS) optimized for open charm meson detection with the CBM - vertex detector, University of Frankfurt/Main and of Strasbourg, March 2008.

[11] M.Winter et al., EUDET-Memo-2007-55: "JRA1-Milestone", 2007. *http://www.eudet.org/e26/e28/e182/e591/eudet-memo-2007-55.pdf*